

Received June 28, 2020, accepted June 30, 2020, date of publication July 3, 2020, date of current version July 16, 2020.

Digital Object Identifier 10.1109/ACCESS.2020.3006914

Landslide Detection Using a Saliency Feature Enhancement Technique From LiDAR-Derived DEM and Orthophotos

BISWAJEET PRADHAN^{1,2}, (Senior Member, IEEE), HUSAM A. H. AL-NAJJAR¹, MAHER IBRAHIM SAMEEN¹, MUSTAFA RIDHA MEZAAL³, AND ABDULLAH M. ALAMRI⁴

¹Centre for Advanced Modelling and Geospatial Information Systems (CAMGIS), Faculty of Engineering and IT, University of Technology Sydney, Sydney, NSW 2007, Australia

²Department of Energy and Mineral Resources Engineering, Sejong University, Seoul 05006, South Korea

³Surveying Department, Institute of Technology-Baghdad, Middle Technical University, Baghdad 11362, Iraq

⁴Department of Geology and Geophysics, College of Science, King Saud University, Riyadh 11362, Saudi Arabia

Corresponding author: Biswajeet Pradhan (biswajeet.pradhan@uts.edu.au)


This work was supported in part by the Centre for Advanced Modelling and Geospatial Information Systems (CAMGIS), University of Technology Sydney (UTS), under Grant 321740.2232335, Grant 321740.2232357, Grant 321740.2232424, and Grant 321740.2232452, and in part by the King Saud University, Riyadh, Saudi Arabia, through the Researchers Supporting Project under Grant RSP-2020/14.

ABSTRACT This study proposes a new landslide detection technique that is semi-automated and based on a saliency enhancement approach. Unlike most of the landslide detection techniques, the approach presented in this paper is simple yet effective and does not require landslide inventory data for training purposes. It comprises several steps. First, it enhances potential landslide pixels. Then, it removes the image background using slope information derived from a very high-resolution LiDAR-based (light detection and ranging) digital elevation model (DEM). After that, morphological analysis was applied to remove small objects, separate landslide objects from each other, and fill the gaps between large bare soil objects and urban objects. Finally, landslide scars were detected using the Fuzzy C-means (FCM) clustering algorithm. The proposed method was developed based on datasets acquired over the Kinta Valley area in Malaysia and tested on another area with a different environment and topography (i.e., Cameron Highlands). The results showed that the proposed landslide detection technique could detect landslides in the training area with a Prediction Accuracy, Kappa index, and Mean Intersection-Over-Union (mIOU) of 71.12%, 0.81, and 68.52%, respectively. The Prediction Accuracy, Kappa index, and mIOU of the method based on the test dataset were 65.78%, 0.68, and 56.14%, respectively. These results show that the proposed method can be used for landslide inventory mapping and risk assessments.

INDEX TERMS Landslide detection, saliency feature enhancement, remote sensing, GIS, LiDAR.

I. INTRODUCTION

Landslide is a destructive natural geohazard that poses significant damage to human life and property every year worldwide, for instance, 187 casualties were recorded by landslide events in Iran, imposing US\$ 12,700,000 up to September 2007 [1]. A landslide in Northern Iran caused a huge loss in infrastructure estimated to be US\$ 5,000,000 in January 2007 [2]. In Malaysia, from 1973 to 2007, landslides caused losses of approximately one Billion US\$ for the period from 1973 to 2007 with over 100 deaths [3]. It is defined as

The associate editor coordinating the review of this manuscript and approving it for publication was Weimin Huang .

a mass movement under of gravity of earth, debris, or rock down a slope [4]–[6]. Even though preventing natural disasters is impossible, great efforts have been put into reducing their impact on society [7]. The preparation of landslide inventory maps is the basic step for landslide susceptibility mapping, hazard and risk assessment [8]. Landslide inventory maps show locations, along with attribute information, of landslides that occurred in a particular area [9]. Nevertheless, these sorts of complete inventory data do not always exist (i.e. impacts of landslides). A complete landslide inventory database contains precise locations, type, and volume of mobilized materials, date of occurrence, and the impacts of past landslides. In contrast, an incomplete landslide inventory

database shows only the location of past landslides that have occurred in an area. The traditional way of landslide mapping is the interpretation of aerial photographs and field surveys. However, with the advancement of remote sensing systems such as very high-resolution satellite sensors and laser scanning systems, landslide mapping has been changed to include automated procedures and a large area mapping in relatively short times [8], [10]–[12].

The current approach consists of (i) Enhancement of potential landslide pixels, (ii) Removing image backgrounds using slope information, (iii) Removing small objects and separating landslide objects from non-landslide objects via morphological analysis, and (iv) Identifying landslide scars by Fuzzy C means (FCM) clustering method. The main contribution of this research is to evaluate the integration of the above methods in a framework that can detect landslides with limited or no inventories data.

The remainder of this article is organized as follows: Section II summarizes the related studies. Section III explains the proposed framework and methodology. Sections IV describes the experimental results. Section V provides the discussion. Lastly, section VI includes the conclusion and suggested future works.

II. RELATED STUDIES

In recent years, several techniques and algorithms have been proposed for landslide mapping using remotely sensed data. The most popular methods are based on object-based image analysis (OBIA) and pixel-based change detection [13]. The basic concept of OBIA methods is the delineation of colour, space, texture, and context at the object level and uses them for the detection of landslide scarps. Reference [14] presented an OBIA-based method for landslide detection in high-resolution, Resourcesat-1 Linear Imaging, and Self Scanning Sensor IV (5.8 m) multispectral image. The method accurately detected five types of landslides with an overall recognition accuracy of 76.9%. Reference [15] proposed a semi-automatic OBIA approach for landslide detection using SPOT images and a digital elevation model (DEM). The method was validated by Persistent Scatterer Interferometry and their results were promising. Moreover, [16] developed an object-oriented landslide detection approach using high-resolution satellite images. They showed that their method could be effectively applied to areas with similar environments. Reference [17] presented an automatic case-based reasoning approach for landslide detection. In their method, OBIA concepts and genetic optimization were integrated to achieve their goal. In their work, the integrated method outperformed the traditional OBIA method reaching from 75% to 87%. Although OBIA methods can achieve reasonable accuracies in landslide mapping, they have some limitations such as segmentation optimization [14], transferability, and scale dependency [14], criteria for the optimal selection of remote sensing data [18] and shadow shortcoming in visual interpretation using NDVI (normalized difference vegetation index) and 3D digital stereoscopy for mapping [19].

Besides, landslide mapping by change detection methods requires multi-temporal remotely sensed data. For instance, [11] improved the landslide classification based on change detection in landslide events using a semi-automatic technique. They implemented a maximum likelihood probability task and a multi-threshold strategy using an automatic histogram division. The evaluation of the EI (Error Index) for three approximations, namely T-global, T-grid, and T-SU (Slope Unit) was carried out with metrics of 0.512, 0.510 and 0.487, respectively. The result showed that SU outperformed the regular grid results. The strategy improved the presentation of the landslide characterization with constrained training samples. However, the transferability of the technique was required. In another study, [20] developed a landslide inventory mapping method using change detection and image fusion technique. They used SPOT and IKONOS images to detect landslides at the regional scale. Their results indicated that the proposed method could achieve 70% accuracy. Furthermore, [21] proposed an object-based change detection method for landslide inventory mapping; the method achieved an accuracy of 81.8% applied to very high-resolution optical images. Reference [22] developed a local similarity measure for landslide detection and compared the results with the image differencing method; the method showed to be more reliable than the simple image differencing method. These methods required bitemporal satellite images, which are difficult to obtain in some areas such as tropical regions or require multi-scans of point clouds (e.g. multi-view), which are often very expensive and not practical. Subsequently, [23] developed a new technique based on saliency enhancement and morphological operations for landslide detection in large areas; the method was carried out using Landsat images acquired over Central Nepal and it performed reasonably well by detecting 99.1% of the landslides in the image; however, the authors indicated that more statistical methods should be developed to accurately separate background objects from landslide regions.

In another study, [24] developed a rule-based semi-automated approach for detection of landslides in Himalaya. The authors used IRS LISS3 satellite images by implementing decision tree methods; the results showed that the overall accuracy of the training and test areas were 76% and 75%, respectively. In another work [11], separating the riverbank from the background object to avoid misclassification of the riverbank was carried out. Authors in another research [25] classified shallow landslides from a high-resolution multi-spectral image and topographic data using a Bayesian framework; the framework was employed to enhance landslide mapping in Southern Taiwan, showing some advantages compared to other semi-auto and automatic approaches [8]. In the last decade, optical images, DEM, and LiDAR data have been used extensively in developing reliable algorithms for landslide detection. However, in recent years, LiDAR data is being more attractive due to its advantages over other data sources. Reference [26] compared LiDAR and aerial photographs for landslide detection. Their analysis showed that LiDAR is

highly effective for accurate landslide delineation, is easier to interpret than aerial photographs, and is highly manipulatable concerning shadows and vertical exaggeration [27] evaluated the suitability of an aerial laser scanner for generating an optimal DTM for mapping landslides in the Cameron Highlands, Malaysia. Authors in [28] reviewed the use of LiDAR for landslide investigations. They discussed the feasibility of using accurate DEMs in landslide applications and inventory mapping. They pointed out that LiDAR data provides promising information for landslide scarps and displaced materials. Accordingly, geomorphological features derived from LiDAR-based DEM (scarps, mobilized materials and foot) can improve the mapping of landslide locations and characteristics.

In tropical areas, several methods based on LiDAR data were proposed for landslide detection. Authors in [29] developed an automated method for detecting landslides using LiDAR data and geomorphological indicators. They used the surface roughness index, the vegetation index, and break lines as indicators for landslide scarps in the study area; their results showed that the best spatial resolution of DEM is 2 and 3 m. Reference [30] presented an expert-based semi-automated method for geomorphological mapping in a mountainous area using LiDAR-based DEM. The authors found that high-resolution DEM is useful for extracting features that are important for landslide mapping in tropical areas. Reference [31] presented a data fusion technique using wavelet transform and Taguchi optimization for landslide detection in a tropical area. Weitao Chen *et al.* [32] developed a framework for landslide detection in Three Gorges, China utilising features derived from LiDAR such as mean aspect, DTM, slope textures, standard division filter of aspect. The features were combined with the Random Forest algorithm, causing a reduction in features set by 74% and improving the overall accuracy of the model by 0.44%. Tao Chen *et al.* [33], used the same reduction strategy, identifying significant landslide features (26 out of 124 features) and then integrated the model with mathematical morphology analysis to map the landslide locations; however, some uncertainties in the segmentation process and tuning parameters were reported. More recently, [34]–[36] used optimization techniques to detect landslides in dense vegetation regions using very high-resolution LiDAR data. The LiDAR data and QuickBird satellite images were fused to detect landslides using the OBIA. The method achieved an overall accuracy of 90.06%, with 65.65% accuracy before fusion.

Despite the success of the landslide detection methods above, they have limitations such as (1) the need of a complete inventory data, which are not always accessible, and (2) they are an expensive and time-consuming process. 2) landslide types and their triggering factors vary from one area to another and different environment achieves relatively lower accuracy in most cases. 3) For accurate landslide detection, segmentation optimization [14] and transferable rules are necessary. 4) Refinement of OBIA rule-sets and other supervised landslide detection methods often require an adequate

number of training landslides to avoid the problem of over-fitting and to improve the generalization capacity of the method [37]–[40].

The current study attempts to develop a quick and practical technique for landslide detection, especially when inventories are scarce or not available. The proposed technique does not require landslide inventory data in the training process and is computationally more efficient than the presented methods especially in emergency cases [23]. Thus, the main aim of this paper is to introduce the efficiency of the presented landslide detection technique and evaluate its performance with different datasets.

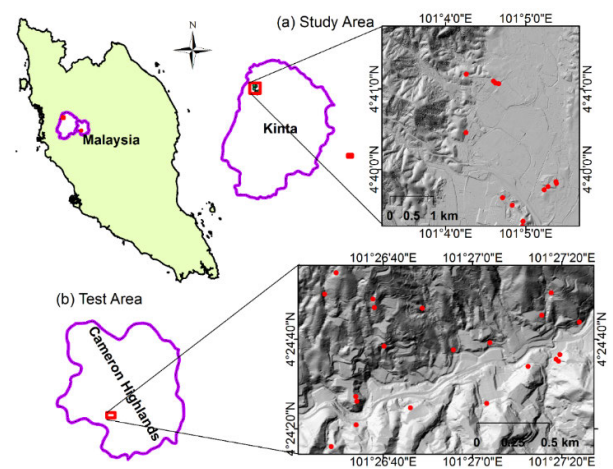


FIGURE 1. The location of the study area used (a) to develop the landslide detection technique and (b) test is used to validate the proposed technique. Besides, red dots represent the landslide locations for both areas.

III. METHODOLOGY

A. STUDY AREA

In this research, the training area was selected in Kinta Valley, located in Perak state, East of Malaysia (Fig.1). It is about 200 km north of Kuala Lumpur. Geographically, it is bounded between $103^{\circ} 3' 5''$ E and $101^{\circ} 5' 47''$ E latitudes and $4^{\circ} 39' 11''$ N and $4^{\circ} 41' 53''$ N longitudes. The area is classified as the tropical rainforest and the temperature is the same with little variations throughout the year with an average temperature of 28°C (Meteorological Service Department of Malaysia). The area sees high rainfall throughout the year with an average of 200 mm each month and the average annual rain is 2428 mm. The region is susceptible to landslides and rockfall because of the loose sands and soft clays in the mining areas [41]. The land use map of the area shows that it includes residential, commercial, and industrial buildings, forest, mixed-grass, and open lands, as well as other infrastructures such as roads, power stations, and drainage sewers.

The test area was selected in the Cameron Highlands, which is 90 km away from the training area. Approximately 80% of the area is forest land, and it has an undulating topography, which makes it effective for performance assessment of the landslide detection models. The average altitude of the

TABLE 1. The details of the data acquisition for the training and test areas.

Specifications	Training area	Test area
Coverage (km ²)	17.25	2.65
System	Airborne system (RIEGL)	Airborne system (RIEGL)
Flight height (m)	1000	1510
Date of acquisition	June 18, 2015	January 15, 2015
Point spacing (pts/m ²)	10	8
Absolute accuracy (m)	0.15	0.15

test area is 1,200 m above the mean sea level, and the total land area is 2.65 km² (Fig. 1). The geology of the Kinta Valley consists of a high percentage of igneous rocks, sedimentary (limestone) and metamorphic rocks (marble).

B. DATASET USED

This research used LiDAR data as the main source for deriving the digital elevation models and slope angle parameters for the training and test area. The details of the data acquisition for both areas are given in Table 1. Additionally, the landslide inventories which are needed for validation purposes were obtained and implemented through remote sensing techniques and technical researches according to previous studies for Kinta Valley and entire Malaysia. The data was collected from archive data of the Mineral and Geoscience Department of Malaysia [42]–[44]. A total of 13 and 21 landslides were identified in the training and test areas, respectively.

C. THE PROPOSED LANDSLIDE DETECTION TECHNIQUE

The proposed landslide detection technique and its performance evaluation and transferability assessment consist of three steps of data processing, as shown in Fig. 2. The first step included data acquisition. The second step was data pre-processing where the input data were prepared for analysis. In this step, LiDAR point clouds, orthophotos and the landslide inventories were geometrically corrected based on the Malaysian GDM 2000 coordinate system to ensure a proper analysis and validation task. Then, a very high-resolution DEM (0.5 m) was produced from the point clouds using the multi-scale curvature algorithm of ESRI’s ArcGIS 10.2 software [45]. In the last step of data pre-processing, a raster map that contains the terrain slope angle, pixel-by-pixel was derived from the LiDAR-DEM with the same spatial resolution. The third step (landslide detection) method consists of four main steps including (1) image saliency enhancement, (2) image background removal, (3) morphology analysis, and (4) Fuzzy C-means (FCM) clustering. None of these steps needs supervision, thus no landslide inventories were used directly in training and developing the model. The available inventory data was only used for validation purposes. The first stage (image saliency enhancement) converted the orthophotos into a new image where the landslide features

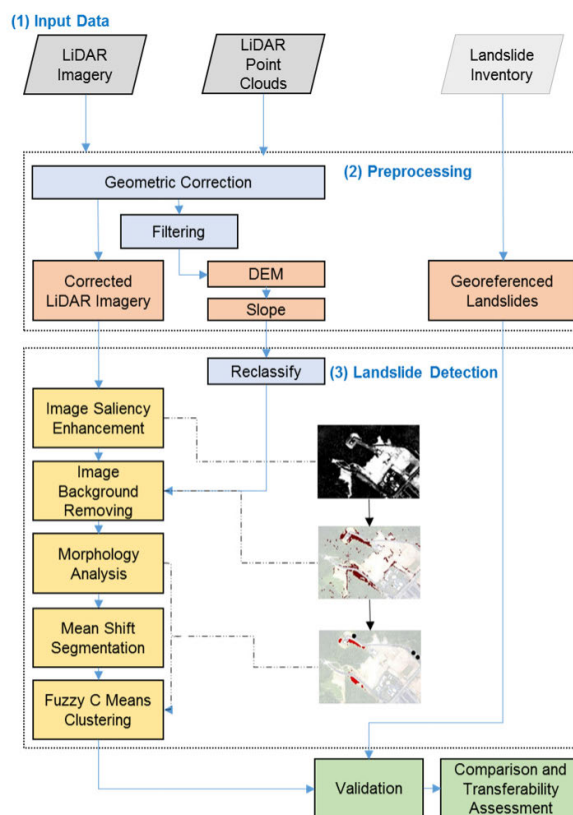


FIGURE 2. The overall flowchart of the proposed landslide detection based on feature saliency enhancement.

were enhanced using the symmetric surrounding regions [46]. The second stage removed the image backgrounds (non-landslide regions) using slope information of the study area as an auxiliary step for the detection process. In this step, the slope map was reclassified into two classes, with slope either above or below 25°. This indicator (threshold) was selected based on practical research in the same study area which referred that a slope above 25 degrees triggers landslides in the region [47]. The value of this threshold is region dependent, so it is expected that the transferability over the new test area may affect the validation accuracy.

In addition, the morphology analysis included a three-time iteration of dilating operation to remove small features and fill the gaps in the large non-landslide regions [48]. Dilating and eroding are two essential tasks of mathematics morphology to structure some compound activities and bring some viable morphology calculation [49]. After that, the FCM unsupervised clustering method was applied to classify the result into landslides and non-landslides where the label of the classes was determined based on orthophoto interpretation. There are two key parameters used in FCM clustering: the fuzzy exponent (m), which defines the fuzziness among each cluster; and (C) which is the number of clusters, which specifies the total number of clusters to be used. The combination of the two parameters affects the results of FCM clustering. The values of FCM clustering parameters were selected based on preliminary examination and previous landslide studies

[50], [51] these parameters were selected as $m = 1.9$ and $C = 3$. Nevertheless, sometimes there are no optimal values for these parameters [50], [50]. Finally, the landslide detection technique was evaluated based on some statistical evaluations and its transferability to another area was investigated.

D. IMAGE SALIENCY ENHANCEMENT

Within the existence of urban features, it is difficult to separate between uncovered soil and urban highlights utilizing just spectral details. Also, the pixel-based examination frequently cannot precisely recognize landslide zones in the image. Notwithstanding, since particular landslides happen in uncovered (bare) soil areas, it can boost this area over urban features so that the identification process may succeed more efficiently via the pixel-based approach. This examination received a saliency improvement approach dependent on the most extreme symmetric surround which is developed by [50]. This method is mainly used to enhance non-vegetation regions, in particular, the bare soil areas of the current study area. The key advantage of this method is that it retains well-defined boundaries by preserving more frequent content from the original image. Other advantages involve in the implementation, simplicity and computational efficiency, particularly at emergency conditions that need a quick response [23], [50].

This saliency algorithm uses surround regions that are symmetric in pixels for which saliency needs to be computed. The advantage of doing so is that each pixel is treated to be at the centre of its sub-image (Fig. 3).

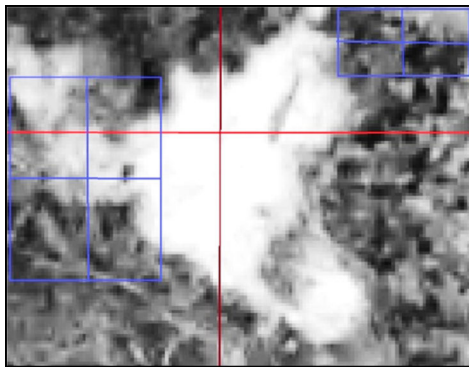


FIGURE 3. Symmetric surround saliency computation concept (red colour: pixel at the centre, blue colour: the kernel which can be elsewhere in the image).

For the orthophotos, the symmetric surround saliency value for a given pixel $S_{ss}(x, y)$ is obtained from the (1) as per the reference [46]:

$$S_{ss}(x, y) = \|I_{\mu}(x, y) - I_f(x, y)\| \tag{1}$$

where $I_{\mu}(x, y)$ is the average value of the CIELAB vector of the sub-image and $I_f(x, y)$ is the corresponding CIELAB image pixel vector in the Gaussian filtered version of the original image computed using (2):

Note: CIELAB is a popular colour space to measure numerical changes in values of transitive and reflective

TABLE 2. The slope statistics of the inventory data of the training and test areas.

Statistics	Training area (Kinta Valley)	Test area (Cameron Highlands)
# Observations	13 landslide locations, 85067 pixels	21 landslide locations, 604911 pixels
Mean slope	27.54	26.72
Std. slope	12.72	15.90
Min. slope	0.38	2.76
Max. slope	46.91	54.79

objects.

$$I_{\mu}(x, y) = \frac{1}{A} \sum_{i=x-x_0}^{x+x_0} \sum_{j=y-y_0}^{y+y_0} I(i, j) \tag{2}$$

where $x_0, y_0,$ and $A,$ are the offsets and area of the sub-image and computed using the following expressions:

$$\begin{aligned} x_0 &= \min(x, w - x) \\ y_0 &= \min(y, h - y) \\ A &= (2x_0 + 1)(2y_0 + 1) \end{aligned} \tag{3}$$

where w and h are the image width and height, respectively. Further details about the algorithm can be realized withing reference [46].

E. SLOPE-BASED IMAGE BACKGROUND REMOVAL

Each geographical location has particular predominant factors causing instability such as curvature, type of soil, man-made activities, etc. [52]. The significance of each factor (e.g. slope) varies with the other factors [2], [7], [53]. The slope of prone areas often plays an essential role in landslides occurrence. Accordingly, the slope raster map can be involved as an indicator to separate the landslide region from other bare soil regions. Several studies on the same study area suggested that regions with a slope higher than 25° are highly prone to landslides [47], [54], [55]. Therefore, the current study reclassified the slope map into a binary raster (0, 1) using the slope indicator of 25° as high prone-landslide areas; 0 indicates the other bare soil regions and 1 indicates the landslide regions. Subsequently, the non-landslide regions were removed as much as possible. Additional information about slope statistics in the training and test areas such as mean, standard deviation (SD), minimum, maximum, and range are provided in Table 2. Moreover, Fig.4 shows the slope distribution in both training and test areas.

F. LANDSLIDE DETECTION WITH MORPHOLOGICAL AND FCM CLUSTERING

In the two previous steps, we attempted to separate landslide regions from other bare soil and urban regions. However, there are still many objects that are not of interest, and they should be removed. This step requires geoscience expertise about landslide objects so that they visually can be differentiated from other non-landslide objects. In other words, bare

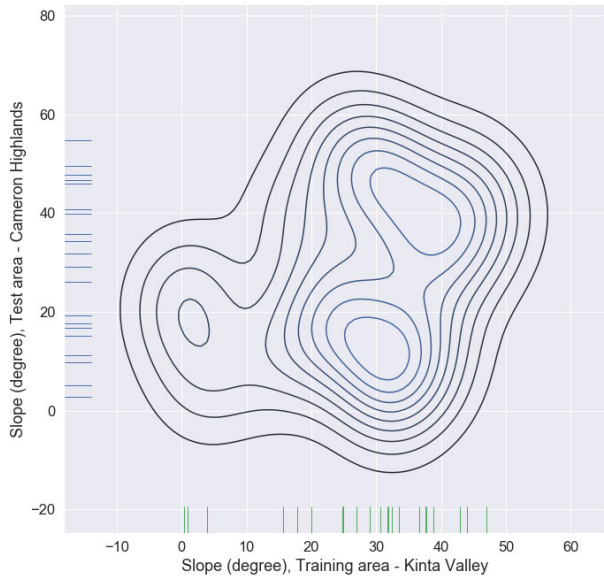


FIGURE 4. Slope distribution in the training (Kinta Valley) and test (Cameron Highlands) areas.

soil and urban objects have relatively large areas, whereas landslides are often small in area, in which these two objects could be distinguishable from each other. Considering this fact, a three-time iteration of a dilating operation with a structural element of 11×11 pixels was applied to further remove non-landslide regions from the result. After that, the generated raster was segmented using the mean shift algorithm [56] and the attributes (i.e. colour, standard deviation, compactness, area) of each object were calculated.

The mean shift technique is a nonparametric technique originally presented by [57] for the calculation of modes in a multivariate of the likelihood function. It was extended to a mode estimation of the joint spatial and spectral domain [58]. In this technique, the Gaussian kernels are usually chosen in most applications [59]. In this stage, this algorithm was selected due to its popularity and main advantages over other algorithms including well-performing with different remote sensing data including medium to very-high-resolution, multivariate nature, simplicity of the filtering steps, flexibility and availability in different implementations [60], [61]. At the end of the process, each pixel is assigned the estimated spectral signature and spatial location of the local mode of the probability density function it belongs to. Finally, the objects were automatically classified into two classes using the FCM clustering method [62], [63]. The landslide objects were labelled using the visual interpretation of LiDAR imageries.

G. PERFORMANCE EVALUATION

The detection accuracy of the proposed method was measured based on four commonly used statistical measures, namely, Overall Accuracy (OA), Prediction Accuracy (PA), Kappa Index, and Mean Intersection-Over-Union (mIOU).

The OA measures the accuracy of the method by comparing the number of landslides or the number of landslides

pixels in the map produced by the proposed method and the number of landslides or the number of landslides pixels in the ground truth data [64]. This measure is a rough accuracy estimate, as it does not account for false detections or spatial agreement. OA was calculated based on (4).

$$OA = \left[1 - \left(\frac{\text{No. Method} - \text{No. Inventory}}{\text{No. Inventory}} \right) \right] \times 100\% \quad (4)$$

where No. The method is the number of landslides or the number of landslide pixels in the result of the proposed method and No. Inventory is the number of landslides or the number of landslide pixels in the inventory data.

The PA and Kappa index are the measures that account for incorrect predictions, and they are a form of reliability measure. A value of $PA = 1$, Kappa index = 1 indicates a perfect performance for the landslide detection method.

The PA and Kappa Index were calculated using the following expression:

$$PA = \frac{TP + TN}{TP + TN + FP + FN} \quad (5)$$

where the TP (true positive) value is the number of pixels that have been predicted correctly as “landslide”, the FP (false positive) value is the number of pixels that have been predicted incorrectly as “landslide”, the TN (true negative) value is the number of pixels that have been predicted correctly as “non-landslide”, and the FN (false negative) value is the number of pixels that have been predicted incorrectly as “non-landslide”.

$$Kappa = \frac{P_p - P_{exp}}{1 - P_{exp}} \quad (6)$$

where, P_p is the proportion of pixels that have been classified correctly as landslide or non-landslide, and P_{exp} means the expected agreements [65]. Furthermore, while none of the methods above measures the spatial agreement between the detection map and the ground truth, this research also used the mean intersection-over-union (mIOU) approach which is widely used in segmentation studies to further assess the performance of the proposed method. The $mIOU = 1$ indicates a perfect prediction and greater than 0.5 is normally considered a “good” prediction [66]. mIOU was computed using (7) [67].

$$mIOU = \frac{1}{k + 1} \sum_{i=0}^k \frac{P_{ii}}{\sum_{j=0}^k P_{ij} + \sum_{j=0}^k P_{ji} - P_{ii}} \quad (7)$$

where $k + 1$ ($k = 1$ in this research) is the number of classes, i is the label of the ground truth, and the j is the label of the prediction. The P_{ij} is the total number of pixels labelled as j but predicted as i .

IV. EXPERIMENTAL RESULTS

A. RESULTS OF LANDSLIDE DETECTION

Fig. 5 shows the result of an initial image saliency enhancement process (Fig. 5a) and after classifying the enhanced image into two classes (Fig. 5b) indicating the initial

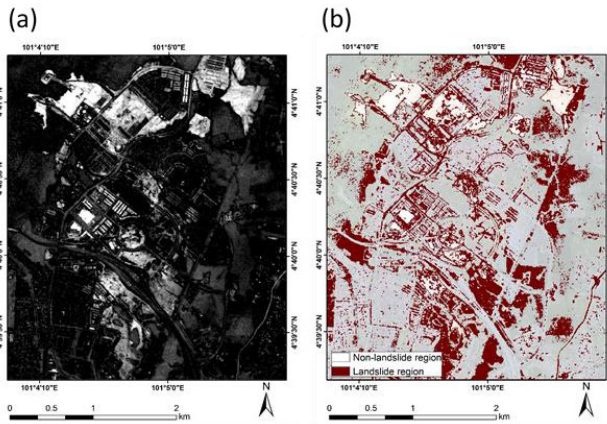


FIGURE 5. Enhanced landslide regions using saliency enhancement applied on orthophotos, (a) after the saliency enhancement process, and (b) after classifying into two classes with the selected threshold.

landslide regions. It can be seen that in orthophotos, after application of saliency enhancement, the contrast of the bare soil and urban regions was enhanced, whereas for vegetated land the contrast was subdued (muted). To separate the potential landslide regions from other regions, the result of image saliency enhancement was classified into two classes with the threshold of 0.54 - 1.75% selected by the quantile classification scheme (which is suitable for ordinal data or ranking) utilising Arc GIS software addressed by [34] (Fig. 5b). This threshold may differ in other areas and data sets; however, it can be automatically selected using common classification algorithms such as quantile, natural breaks, or others [68]. With additional geoscience knowledge about the landslide in the study area, this threshold can be further optimized to reduce the miss-classification between the landslide regions and other bare soil and urban regions. The initial landslide region contained many objects belonging to the bare soil and urban areas from where they needed to be removed.

To remove the misclassified bare soil and urban objects as landslides, the slope raster layer was used. As it was referred previously, in the study area of this research objects with a slope of less than 25° were removed as there is a very low possibility for these to be subject to the landslide event; this was addressed by a recent study for the same area by [47]. The results of this process are shown in Fig. 6. The slope of the study area ranged from 0 to $\sim 83^\circ$ where the highest slopes were found in the northwest part of the area. These areas are mostly forest and cliffs. After removing the regions with a slope of less than 25° , the result showed that potential landslides were mostly in the south and northwest parts of the study area (Fig. 6). However, the resulting map contained many small objects distributed over the study area and needed further processing, which is discussed in the following section. The values of this slope threshold contributed to separating landslides from other land cover classes such as bare soil. It can be credited to the characteristics of a landslide in the area under consideration. This indicates

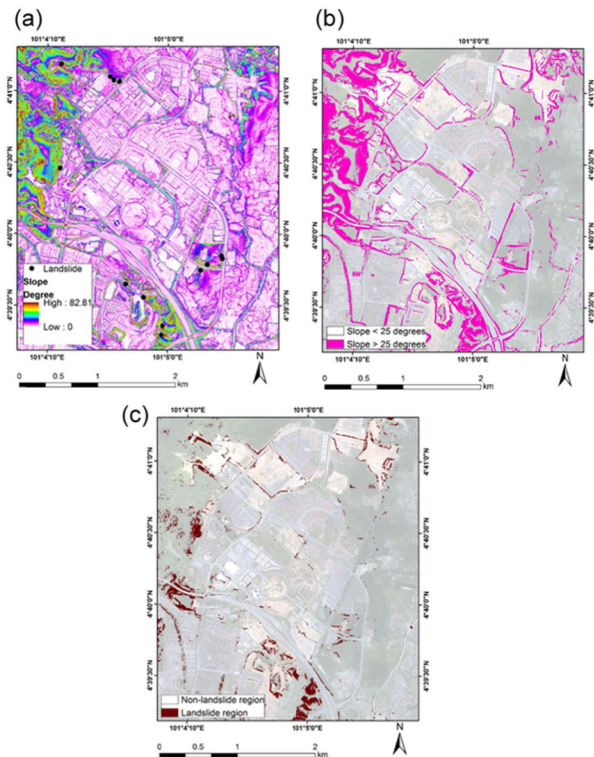


FIGURE 6. The identified landslide regions after removing image background by the reclassified slope map, (a) slope map, (b) slope map after reclassification, and (c) result of identified landslides after slope-based enhancement.

that the LiDAR-derived data and orthophotos are efficiently operative in revealing the location of landslide.

The dilate operation with a structural element of 11×11 pixels as a morphological processing step was employed to refine the landslide detection result. The landslide regions detected after morphological processing are shown in Fig. 7a. Overall, 120358.82 m^2 (0.97% of total area) were detected as landslides (shown in red colour). After that, the generated raster was segmented using the mean shift algorithm [55] and the optimal segmentation parameters (i.e. scale, shape, and compactness) were calculated. The general goal of this segmentation is to partition an image into semantically meaningful regions. This can be accomplished by clustering the pixels in the image using a Gaussian kernel [59] (Fig. 7).

Considering the great diversity of landslides, environmental settings and accessible images, feature selection in high-dimensional datasets is a significant task which was recommended by previous landslide detection researches to target a better performance of data classification [33], [69], [70].

To obtain the optimum features [32], [70], correlation-based feature selection was used to select the most important features for identifying landslide locations with 20 iterations. The total input features contained 82 features derived from LiDAR data (height, slope, and intensity), texture features (GLCM homogeneity and GLCM StdDev), and the

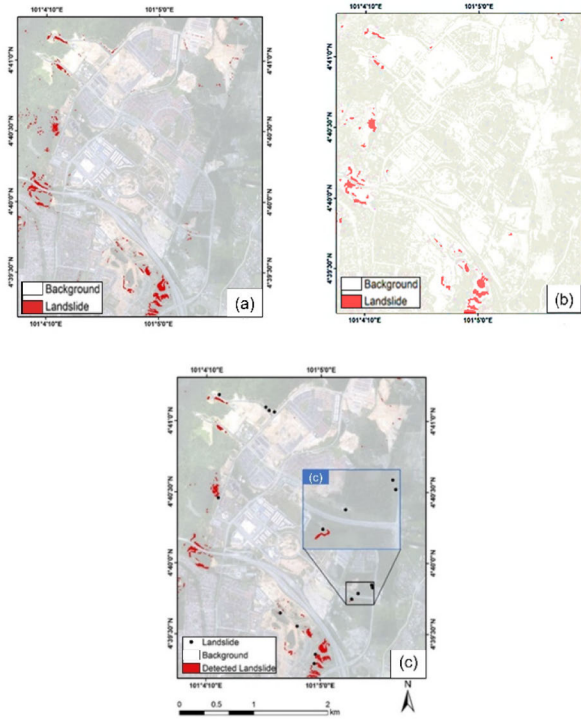


FIGURE 7. Results of landslide detection, (a) detected landslide regions after the dilate operation, (b) result of mean-shift segmentation, and (c) result of landslide detection of the training area.

TABLE 3. Results of selected features used in this study.

Most important features in this study				
(1) Mean Intensity	(2) GLCM Homogeneity	(3) Mean Slope	(4) GLCM Angular Second Moment	(5) StdDe DTM
(6) Mean Red	(7) Mean DTM	(8) GLCM Contrast	(9) GLCM Dissimilarity	(10) GLCM Dissimilarity

visible band. The highest accuracy was achieved when the features were reduced to 10 features (most important features). Table 3 represents the most important features selected for this study. The values of these features were contributed to separate landslides from other land cover classes.

The result was further refined using the FCM clustering method, where the objects were automatically classified into two classes using spectral and spatial attributes. The result is shown in Fig. 7c. The overall area of landslide regions was 64780.95 m², which was only 0.52% of the study area. Also, the number of detected landslides was 17. The minimum and maximum areas of the detected landslides were 111 and 11147.29 m², respectively.

B. PERFORMANCE EVALUATION

The comparison of the number of landslides and the number of landslide pixels between the inventory data and the result of the proposed technique is shown in Table 4. The landslide

TABLE 4. Comparison between the number of landslides and landslide pixels between the inventory data and the result of the proposed technique.

Interest area	Details	Inventory data	Proposed technique	Accuracy
Training area	Number of landslides	13	17	69.23%
	Number of landslide pixels	85067	98125	84.64%
Test area	Number of landslides	21	37	28%
	Number of landslide pixels	604911	858973	58%

inventory data of the training area had 13 landslide locations. The number of landslides detected by the proposed method was 17. Therefore, the accuracy was calculated as 69.23%.

With a simple but computationally efficient method, an accuracy of 69.23% in terms of detecting the number of landslides seems acceptable, given that no inventory data were used for the detection process compared to traditional and other methods proposed in the literature. Additionally, the number of landslide pixels in the inventory data of the training area was calculated as 85067 for 13 landslide objects, whereas for the detected landslides the number of landslide pixels was 98125. This resulted in an accuracy of 84.64% for the proposed technique using the training area. On the other hand, the test area contained 21 landslide locations and 604911 landslide pixels. The number of landslides and landslide pixels detected in the test area by the proposed method was 37 and 858973, respectively. Thus, the calculated accuracy for the detection of the number of landslides and landslide pixels was 28% and 58%, respectively.

In addition, Table 5 shows the accuracy assessment using a landslide inventory data containing 13 landslide locations of the training area and 21 of the test area and statistical evaluation indices. The performance of the landslide detection technique was evaluated using PA, Kappa index, and mIOU. For the training area, the PA, Kappa index, and mIOU are 71.12%, 0.81, and 68.52% respectively. However, the PA, Kappa index, and mIOU of the method in the test area are 65.78%, 0.68, and 56.14%, respectively. The lower accuracy of the method on the test area is mainly because the terrain (topography and geomorphology) of the Cameron Highlands area is much more complicated. Additional factors that contributed to lowering the accuracy of landslide detection in the test area included the presence of man-made slopes, which are very similar to natural landslides in terms of spectral and spatial characteristics. Considering prior knowledge about these man-made slopes, more undesirable objects can further be removed from the image, accordingly, and results of the landslide detection might be improved.

Results of the landslide detection for the test area are shown in Fig. 8. The use of the proposed technique promises positive progress in the detection accuracy of landslides,

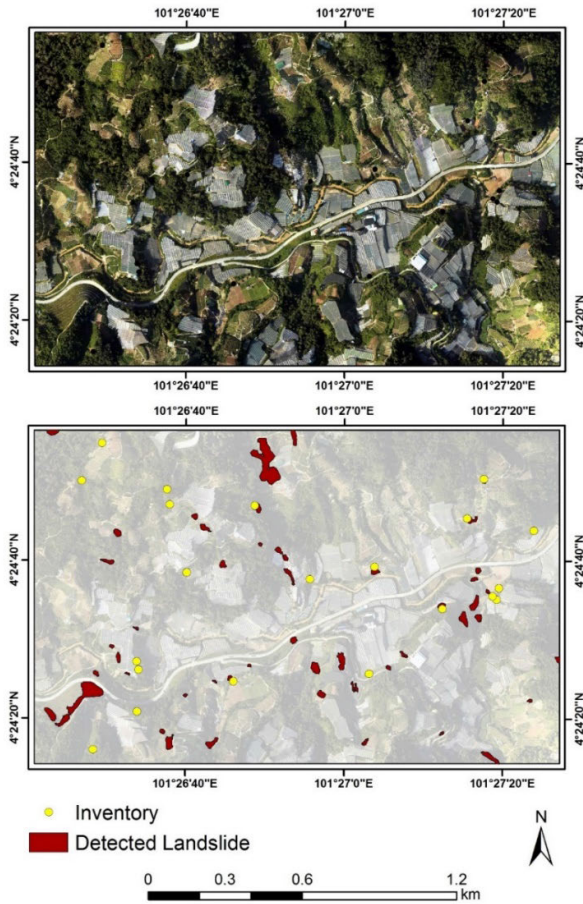


FIGURE 8. Result of landslide detection technique applied to the test area.

TABLE 5. The PA, Kappa index, and mIOU of the proposed technique for the training and the test areas.

Measure	Training area	Test area	Average accuracy
PA	71.12%	65.78%	68.45%
Kappa index	0.81	0.68	0.745
mIOU	68.52%	56.14%	62.33%

especially when inventory data are limited and not available. Moreover, high-resolution LiDAR and visible bands contributed to the simplification in the development of the current research.

V. DISCUSSION

Landslide inventory mapping is an important task in hazard and risk assessments. This study proposed a simple but effective landslide detection technique using the saliency feature enhancement and some other traditional algorithms such as morphological operations, mean shift segmentation, and FCM classification. The main data used are LiDAR-derived slope map and orthophotos and the proposed landslide detection technique could be a useful tool for landslide mapping and monitoring specifically when inventories are scarce as well as there is a need of quick response time.

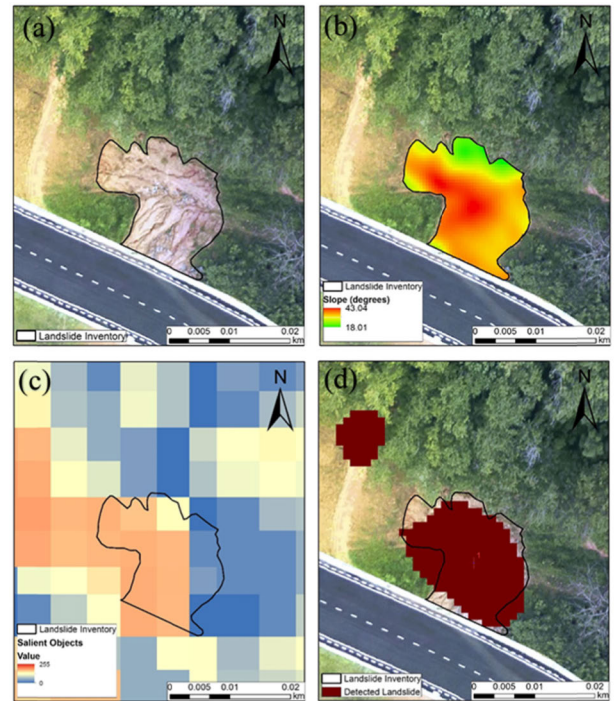


FIGURE 9. Example of a detected landslide by the proposed technique, (a) the manually digitized landslide, (b) the calculated slope for the landslide scar area, (c) the salient landslide objects, and (d) the detected landslide.

Fig. 9 shows one of the landslides detected in the training area (Kinta Valley). The manually digitized landslide and the calculated slope for the landslide body are shown in Fig. 9a and Fig.9b. Also, the salient objects resulting from the saliency enhancement for the area and the final detected landslide by the proposed technique are shown respectively in (Fig. 9c, d). The area of the shown landslide was 295.72 m² surrounded by a highway and dense vegetation. The low slopes can be observed at the top of the landslide (initial source) and the boundary of the landslide scar. In contrast, Fig. 9c shows the enhanced image using the symmetric surround saliency enhancement technique. It can be seen that a large part of the landslide region has gained the highest brightness values (>200) while the surrounding areas had low values with some high values for the unpaved road in the east part of the area. Furthermore, Fig. 9d shows the detected landslide by the proposed method. It can be observed that some pixels have not been detected as landslides because of their low slope value, as shown in Fig. 9b. The overall accuracy of this landslide detection was 87%. This example shows the efficiency of the proposed techniques for landslide mapping and monitoring. However, to improve the accuracy of landslide boundary delineation, further processing and enhancement of the technique are needed.

Different objects of similar spectral characteristics of landslides would largely weaken the detection rate making it hard to meet the requirements for further landslide analysis. In the proposed approach, as most bare soil and urban zones are not of our interest (background/ unwanted objects), the morphology analysis was employed to further remove

and refine these unwanted objects. Using the morphological analysis, the detection process was further improved so that the non-landslide regions were refined (decreased) reaching 0.120 Km², which comprised 0.97% of the total area (Fig 10).

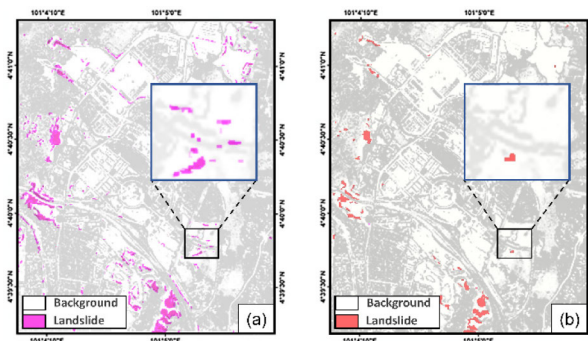


FIGURE 10. Effect of removing the morphological operation to landslide detection, (a) before morphology operation, and (b) after morphology operation.

To evaluate the advantages of this morphology, we further examined the landslide detection by removing the morphological analysis from the main process. It was noticed that by eliminating this step, the presence of unwanted objects was raised by nearly two-fold. Fig. 10a clearly shows that the non-landslide objects were increasingly presented in the analysis, indicating a negative impact on the entire process. This is because the morphological operation provides the value of each pixel in the output image based on a comparison of the matching pixel in the input image with its neighbours to enhance the analysis. Furthermore, the combination of dilation and erosion tasks in the same structuring element provides functions to remove the unwanted/ small objects from an image and smooth the boundary of large objects. It can be inferred that involving the morphology step (Fig. 10b) was a successful strategy taken to separate the landslide and non-landslide regions. This was agreed with suggested studies in [23], [33]. Nevertheless, careful selection of scales and mask dimensions is vital in the design of comprehensive algorithms for all these tasks.

There are numerous features such as spectral, LiDAR-factors, spatial and textural that can be used in OBIA methods, however, when the number of features is more than the number of training samples, over-fitting is more likely to happen [71]. Nevertheless, with many landslide inventory locations, OBIA-methods can be more robust for the following reasons. Data from various sources and scales can be effectively integrated at the object level. They capture the complexity of the natural phenomenon and geomorphologic processes such as landslides better than pixel-based methods. Also, results produced by the OBIA methods contain much less “salt and pepper” noise than pixel-based methods [63]. In general, instead of using landslide inventory data for model training, general knowledge about the study area is often used.

In the current research, the landslide events could be detected using both geomorphological characteristics (i.e.,

slope), as well as assisting the expert’s advice regarding the study area [43], [47], [54], [55], [72]. Even though knowledge representation in computer programming is not an easy task of modelling, the result of this technique could be more generalizable than data-driven techniques.

Despite the advancement of the spatial resolution of DEM and orthophotos, reliable landslide detection from remote sensing data is still challenging. The proposed method resulted in a promising performance, given that no inventories were used in the training process (unlike the traditional methods). It could statistically achieve average accuracies of 68.45% PA, 0.745 Kappa index, and 62.33% mIOU. Compared with other unsupervised detection methods, the average reliability accuracy obtained in this study scored a Kappa index of 0.745, which was higher than [23]. Scientists in a previous study [23] utilized the Landsat 8 image by employing the saliency and morphological analysis, for which the highest Kappa index of 0.42 for training and 0.25 for tests was obtained. In comparison with another unsupervised detection using K-means clustering via slope feature extraction [73], the accuracy of 54.54 for two clusters, and 85.47 for five clusters were obtained; however, misclassification in some landslide locations was reported.

Machine learning methods have a core disadvantage that they need the spatial distribution of the test data to be similar to that of the training data [74]. In data science generally, by having more training data (landslide inventories), better accuracy can be achieved. But because the main contribution of the proposed study is exclusively not to use inventory data in the training processes, the result indicates a convincing prediction ratio, unlike most of the existing methods [16]. This can be considered a justifiable advantage over the traditional methods, especially when the disaster’s response time is the dominant issue, providing a faster way to map regional hazards. Only a few studies have tried to detect landslides without inventory data, similar accuracies were obtained; however, some uncertainties were reported [17].

VI. CONCLUSION

This study introduced a semi-automated landslide detection technique that does not require landslide inventory data for the training purpose and provides a quick practical solution for landslide mapping and monitoring, particularly for emergency conditions and monitoring. The technique used symmetric surround saliency enhancement, morphological operations, mean shift segmentation, and fuzzy-based clustering methods. The experimental results showed that the proposed technique is simple and effective and its average accuracy can reach 71% for areas with complicated topography and geomorphology. The technique performed well both in the training area (Kinta Valley) and the test area (Cameron Highlands) located in a high landslide-prone region in Malaysia.

Overall, the proposed solution of landslide detection using LiDAR-DEM and orthophotos is promising for landslide inventory mapping and landslide monitoring, especially in areas where data is scarce. Despite the acceptable accuracies

achieved for landslide detection by the proposed method, some points need to be improved in future work. First, an optimized combination of RGB and additional bands such as near and shortwave infrared could be used to enhance the geologic features before the saliency enhancement process. Moreover, a combination of landslide factors (e.g slope, altitude, curvature, type of soil) could be utilized as an indicator/threshold to further enhance the background removing process.

REFERENCES

- [1] H. R. Pourghasemi, M. Mohammady, and B. Pradhan, "Landslide susceptibility mapping using index of entropy and conditional probability models in GIS: Safarood Basin, Iran," *Catena*, vol. 97, pp. 71–84, Oct. 2012.
- [2] M. I. Sameen and B. Pradhan, "Landslide detection using residual networks and the fusion of spectral and topographic information," *IEEE Access*, vol. 7, pp. 114363–114373, 2019, doi: [10.1109/ACCESS.2019.2935761](https://doi.org/10.1109/ACCESS.2019.2935761).
- [3] A. Akter, M. J. M. M. Noor, M. Goto, S. Khanam, A. Parvez, and M. Rasheduzzaman, "Landslide disaster in malaysia: An overview," *Int. J. Innov. Res. Develop.*, vol. 8, no. 6, pp. 58–71, Jun. 2019.
- [4] D. M. Cruden, "A simple definition of a landslide," *Bull. Int. Assoc. Eng. Geol.*, vol. 43, no. 1, pp. 27–29, Apr. 1991.
- [5] D. M. Cruden and D. J. Varnes, "Landslide types and processes," *Landslides, Invest. Mitigation*, Bell, Washington, DC, USA, Transp. Res. Board Special Rep. 247, 1996, ch. 3, pp. 36–75.
- [6] Y. Alimohammadlou, A. Najafi, and A. Yalcin, "Landslide process and impacts: A proposed classification method," *Catena*, vol. 104, pp. 219–232, May 2013.
- [7] A. M. Fanos and B. Pradhan, "A novel hybrid machine learning-based model for rockfall source identification in presence of other landslide types using LiDAR and GIS," *Earth Syst. Environ.*, vol. 3, no. 3, pp. 491–506, Dec. 2019, doi: [10.1007/s41748-019-00114-z](https://doi.org/10.1007/s41748-019-00114-z).
- [8] F. Guzzetti, A. C. Mondini, M. Cardinali, F. Fiorucci, M. Santangelo, and K.-T. Chang, "Landslide inventory maps: New tools for an old problem," *Earth-Sci. Rev.*, vol. 112, nos. 1–2, pp. 42–66, Apr. 2012.
- [9] IAEG Commission, "Engineering geological mapping: Classification of rocks and soils for engineering geology mapping. Part 1: Rock and soil materials," *Bull. Int. Assoc. Eng. Geol.*, Krefeld, Germany, Tech. Rep., 1979, vol. 19, pp. 364–371.
- [10] N. Casagli, W. Frodella, S. Morelli, V. Tofani, A. Ciampalini, E. Intrieri, F. Raspini, G. Rossi, L. Tanteri, and P. Lu, "Spaceborne, UAV and ground-based remote sensing techniques for landslide mapping, monitoring and early warning," *Geoenvironmental Disasters*, vol. 4, no. 1, pp. 1–23, Dec. 2017.
- [11] M. Alvioli, A. C. Mondini, F. Fiorucci, M. Cardinali, and I. Marchesini, "Topography-driven satellite imagery analysis for landslide mapping," *Geomatics, Natural Hazards Risk*, vol. 9, no. 1, pp. 1913–1926, 2018.
- [12] K. E. Joyce, S. E. Belliss, S. V. Samsonov, S. J. McNeill, and P. J. Glassey, "A review of the status of satellite remote sensing and image processing techniques for mapping natural hazards and disasters," *Prog. Phys. Geography, Earth Environ.*, vol. 33, no. 2, pp. 183–207, Apr. 2009.
- [13] V. Moosavi, A. Talebi, and B. Shirmohammadi, "Producing a landslide inventory map using pixel-based and object-oriented approaches optimized by taguchi method," *Geomorphology*, vol. 204, pp. 646–656, Jan. 2014.
- [14] T. R. Martha, N. Kerle, C. J. van Westen, V. Jetten, and K. V. Kumar, "Segment optimization and data-driven thresholding for knowledge-based landslide detection by object-based image analysis," *IEEE Trans. Geosci. Remote Sens.*, vol. 49, no. 12, pp. 4928–4943, Dec. 2011.
- [15] D. Hölbling, P. Füreder, F. Antolini, F. Cigna, N. Casagli, and S. Lang, "A semi-automated object-based approach for landslide detection validated by persistent scatterer interferometry measures and landslide inventories," *Remote Sens.*, vol. 4, no. 5, pp. 1310–1336, May 2012.
- [16] D. Y. Hu, J. Li, W. J. Zhao, and G. X. Peng, "Object-oriented landslide detection from remote sensing images with high resolution," *J. Natural Disasters*, vol. 17, no. 6, pp. 42–46, 2008.
- [17] J. Dou, K.-T. Chang, S. Chen, A. Yunus, J.-K. Liu, H. Xia, and Z. Zhu, "Automatic case-based reasoning approach for landslide detection: Integration of object-oriented image analysis and a genetic algorithm," *Remote Sens.*, vol. 7, no. 4, pp. 4318–4342, Apr. 2015.
- [18] F. Fiorucci, D. Giordan, M. Santangelo, F. Dutto, M. Rossi, and F. Guzzetti, "Criteria for the optimal selection of remote sensing optical images to map event landslides," *Natural Hazards Earth Syst. Sci.*, vol. 18, no. 1, pp. 405–417, Jan. 2018.
- [19] F. Fiorucci, F. Ardizzone, A. C. Mondini, A. Viero, and F. Guzzetti, "Visual interpretation of stereoscopic NDVI satellite images to map rainfall-induced landslides," *Landslides*, vol. 16, no. 1, pp. 165–174, Jan. 2019.
- [20] J. Nichol and M. S. Wong, "Satellite remote sensing for detailed landslide inventories using change detection and image fusion," *Int. J. Remote Sens.*, vol. 26, no. 9, pp. 1913–1926, May 2005.
- [21] P. Lu, A. Stumpf, N. Kerle, and N. Casagli, "Object-oriented change detection for landslide rapid mapping," *IEEE Geosci. Remote Sens. Lett.*, vol. 8, no. 4, pp. 701–705, Jul. 2011.
- [22] S. Khairunniza-Bejo, M. Petrou, and A. Ganas, "Local similarity measure for landslide detection and identification in comparison with the image differencing method," *Int. J. Remote Sens.*, vol. 31, no. 23, pp. 6033–6045, Dec. 2010.
- [23] B. Yu and F. Chen, "A new technique for landslide mapping from a large-scale remote sensed image: A case study of central nepal," *Comput. Geosci.*, vol. 100, pp. 115–124, Mar. 2017.
- [24] S. Siyahghalati, A. K. Saraf, B. Pradhan, M. N. Jebur, and M. S. Tehrani, "Rule-based semi-automated approach for the detection of landslides induced by 18 September 2011 Sikkim, Himalaya, Earthquake using IRS LISS3 satellite images," *Geomatics, Natural Hazards Risk*, vol. 7, no. 1, pp. 326–344, Jan. 2016.
- [25] A. C. Mondini, I. Marchesini, M. Rossi, K.-T. Chang, G. Pasquariello, and F. Guzzetti, "Bayesian framework for mapping and classifying shallow landslides exploiting remote sensing and topographic data," *Geomorphology*, vol. 201, pp. 135–147, Nov. 2013.
- [26] R. D. Gold, K. W. Wegmann, S. P. Palmer, R. J. Carson, and P. K. Spencer, "Comparative study of aerial photographs and LiDAR imagery for landslide detection in the Puget Lowland, Washington," in *Proc. 99th Annu. Meeting*, Puerto Vallarta, Mexico, Apr. 2003.
- [27] K. A. Razak, M. Santangelo, C. J. Van Westen, M. W. Straatsma, and S. M. de Jong, "Generating an optimal DTM from airborne laser scanning data for landslide mapping in a tropical forest environment," *Geomorphology*, vol. 190, pp. 112–125, May 2013.
- [28] M. Jaboyedoff, T. Oppikofer, A. Abellán, M.-H. Derron, A. Loya, R. Metzger, and A. Pedrazzini, "Use of LiDAR in landslide investigations: A review," *Natural Hazards*, vol. 61, no. 1, pp. 5–28, Mar. 2012.
- [29] U. Mann, B. Pradhan, N. Prechtel, and M. F. Buchroithner, "An automated approach for detection of shallow landslides from LiDAR derived DEM using geomorphological indicators in a tropical forest," in *Terrigenous Mass Movements*, B. Pradhan and M. Buchroithner, Eds. Berlin, Germany: Springer, 2012, pp. 1–22.
- [30] S. van Asselen and A. C. Seijmonsbergen, "Expert-driven semi-automated geomorphological mapping for a mountainous area using a laser DTM," *Geomorphology*, vol. 78, nos. 3–4, pp. 309–320, Aug. 2006.
- [31] B. Pradhan, M. N. Jebur, H. Z. M. Shafri, and M. S. Tehrani, "Data fusion technique using wavelet transform and taguchi methods for automatic landslide detection from airborne laser scanning data and QuickBird satellite imagery," *IEEE Trans. Geosci. Remote Sens.*, vol. 54, no. 3, pp. 1610–1622, Mar. 2016.
- [32] W. Chen, X. Li, Y. Wang, G. Chen, and S. Liu, "Forested landslide detection using LiDAR data and the random forest algorithm: A case study of the three gorges, China," *Remote Sens. Environ.*, vol. 152, pp. 291–301, Sep. 2014.
- [33] T. Chen, J. Trinder, and R. Niu, "Object-oriented landslide mapping using ZY-3 satellite imagery, random forest and mathematical morphology, for the three-gorges reservoir, China," *Remote Sens.*, vol. 9, no. 4, p. 333, Mar. 2017.
- [34] B. Pradhan and M. R. Mezaal, "Optimized rule sets for automatic landslide characteristic detection in a highly vegetated forests," in *Laser Scanning Applications in Landslide Assessment*, B. Pradhan, Ed. Cham, Switzerland: Springer, 2017, doi: [10.1007/978-3-319-55342-9_3](https://doi.org/10.1007/978-3-319-55342-9_3).
- [35] M. R. Mezaal, B. Pradhan, H. Z. M. Shafri, and Z. M. Yusoff, "Automatic landslide detection using Dempster-Shafer theory from LiDAR-derived data and orthophotos," *Geomatics, Natural Hazards Risk*, vol. 8, no. 2, pp. 1935–1954, Dec. 2017.
- [36] M. R. Mezaal, B. Pradhan, M. I. Sameen, H. Z. Mohd Shafri, and Z. M. Yusoff, "Optimized neural architecture for automatic landslide detection from high-resolution airborne laser scanning data," *Appl. Sci.*, vol. 7, no. 7, p. 730, Jul. 2017.
- [37] H. Shahabi and M. Hashim, "Landslide susceptibility mapping using GIS-based statistical models and remote sensing data in tropical environment," *Sci. Rep.*, vol. 5, no. 1, pp. 1–15, Sep. 2015.
- [38] T. Blaschke, "Object based image analysis for remote sensing," *ISPRS J. Photogramm. Remote Sens.*, vol. 65, no. 1, pp. 2–16, Jan. 2010.

- [39] T. Blaschke, G. J. Hay, M. Kelly, S. Lang, P. Hofmann, E. Addink, R. Q. Feitosa, F. van der Meer, H. van der Werff, F. van Coillie, and D. Tiede, "Geographic object-based image analysis-towards a new paradigm," *ISPRS J. Photogramm. Remote Sens.*, vol. 87, pp. 180–191, Jan. 2014.
- [40] M. D. Hossain and D. Chen, "Segmentation for object-based image analysis (OBIA): A review of algorithms and challenges from remote sensing perspective," *ISPRS J. Photogramm. Remote Sens.*, vol. 150, pp. 115–134, Apr. 2019.
- [41] C. Xu, F. Dai, X. Xu, and Y. H. Lee, "GIS-based support vector machine modeling of earthquake-triggered landslide susceptibility in the Jianjiang River Watershed, China," *Geomorphology*, vols. 145–146, pp. 70–80, Apr. 2012.
- [42] B. Pradhan and S. Lee, "Regional landslide susceptibility analysis using back-propagation neural network model at cameron Highland, Malaysia," *Landslides*, vol. 7, no. 1, pp. 13–30, Mar. 2010.
- [43] B. Pradhan, M. H. Abokharima, M. N. Jebur, and M. S. Tehrani, "Land subsidence susceptibility mapping at Kinta Valley (Malaysia) using the evidential belief function model in GIS," *Natural Hazards*, vol. 73, no. 2, pp. 1019–1042, Sep. 2014.
- [44] A. M. Fanos, and B. Pradhan, "A spatial ensemble model for rockfall source identification from high resolution LiDAR data and GIS," *IEEE Access*, vol. 7, pp. 74570–74585, 2019, doi: 10.1109/ACCESS.2019.2919977.
- [45] J. S. Evans and A. T. Hudak, "A multiscale curvature algorithm for classifying discrete return LiDAR in forested environments," *IEEE Trans. Geosci. Remote Sens.*, vol. 45, no. 4, pp. 1029–1038, Apr. 2007.
- [46] R. Achanta and S. Susstrunk, "Saliency detection using maximum symmetric surround," in *Proc. IEEE Int. Conf. Image Process.*, Sep. 2010, pp. 2653–2656.
- [47] M. Mezaal, B. Pradhan, and H. Rizeei, "Improving landslide detection from airborne laser scanning data using optimized Dempster-Shafer," *Remote Sens.*, vol. 10, no. 7, p. 1029, Jun. 2018.
- [48] D. Hu and X. Tian, "A multi-directions algorithm for edge detection based on fuzzy mathematical morphology," in *Proc. 16th Int. Conf. Artif. Reality Telexistence-Workshops (ICAT)*, Nov. 2006, pp. 361–364.
- [49] R. M. Haralick and S. R. Sternberg, "Image analysis morphology," *Analysis*, vol. 9, no. 4, pp. 532–550, 1987.
- [50] X.-L. Sun, Y.-G. Zhao, H.-L. Wang, L. Yang, C.-Z. Qin, A.-X. Zhu, G.-L. Zhang, T. Pei, and B.-L. Li, "Sensitivity of digital soil maps based on FCM to the fuzzy exponent and the number of clusters," *Geoderma*, vols. 171–172, pp. 24–34, Feb. 2012.
- [51] L.-J. Wang, K. Sawada, and S. Moriguchi, "Landslide susceptibility analysis with logistic regression model based on FCM sampling strategy," *Comput. Geosci.*, vol. 57, pp. 81–92, Aug. 2013.
- [52] D. J. Varnes, "Slope movement types and processes," *Special Rep.*, vol. 176, no. 176, pp. 11–33, 1978.
- [53] D. R. Montgomery and M. T. Brandon, "Topographic controls on erosion rates in tectonically active mountain ranges," *Earth Planet. Sci. Lett.*, vol. 201, nos. 3–4, pp. 481–489, Aug. 2002.
- [54] S. Lee and B. Pradhan, "Landslide hazard mapping at Selangor, Malaysia using frequency ratio and logistic regression models," *Landslides*, vol. 4, no. 1, pp. 33–41, Feb. 2007.
- [55] B. Pradhan, "Use of GIS-based fuzzy logic relations and its cross application to produce landslide susceptibility maps in three test areas in Malaysia," *Environ. Earth Sci.*, vol. 63, no. 2, pp. 329–349, May 2011.
- [56] D. Comaniciu, V. Ramesh, and P. Meer, "The variable bandwidth mean shift and data-driven scale selection," in *Proc. 8th IEEE Int. Conf. Comput. Vis. (ICCV)*, vol. 1, Jul. 2001, pp. 438–445.
- [57] K. Fukunaga and L. Hostetler, "The estimation of the gradient of a density function, with applications in pattern recognition," *IEEE Trans. Inf. Theory*, vol. 21, no. 1, pp. 32–40, Jan. 1975.
- [58] D. Comaniciu and P. Meer, "Mean shift: A robust approach toward feature space analysis," *IEEE Trans. Pattern Anal. Mach. Intell.*, vol. 24, no. 5, pp. 603–619, May 2002.
- [59] J. Michel, D. Youssefi, and M. Grizonnet, "Stable mean-shift algorithm and its application to the segmentation of arbitrarily large remote sensing images," *IEEE Trans. Geosci. Remote Sens.*, vol. 53, no. 2, pp. 952–964, Feb. 2015.
- [60] E. Christophe and J. Inglada, "Object counting in high resolution remote sensing images with OTB," in *Proc. IEEE Int. Geosci. Remote Sens. Symp.*, vol. 4, Jul. 2009, pp. 737–740.
- [61] J. Michel, J. Malik, and J. Inglada, "Lazy yet efficient land-cover map generation for HR optical images," in *Proc. IEEE Int. Geosci. Remote Sens. Symp.*, Jul. 2010, pp. 1863–1866.
- [62] M. Feher and J. M. Schmidt, "Fuzzy clustering as a means of selecting representative conformers and molecular alignments," *J. Chem. Inf. Comput. Sci.*, vol. 43, no. 3, pp. 810–818, May 2003.
- [63] L. V. Tilson, P. S. Excell, and R. J. Green, "A generalisation of the fuzzy C-means clustering algorithm," in *Proc. Int. Geosci. Remote Sens. Symp., Remote Sens., Moving Toward 21st Century*, vol. 10, no. 2, 1988, pp. 1783–1784.
- [64] B. Pradhan, "A comparative study on the predictive ability of the decision tree, support vector machine and neuro-fuzzy models in landslide susceptibility mapping using GIS," *Comput. Geosci.*, vol. 51, pp. 350–365, Feb. 2013.
- [65] N. D. Bennett, B. F. W. Croke, G. Guariso, J. H. A. Guillaume, S. H. Hamilton, A. J. Jakeman, S. Marsili-Libelli, L. T. H. Newham, J. P. Norton, C. Perrin, S. A. Pierce, B. Robson, R. Seppelt, A. A. Voinov, B. D. Fath, and V. Andreassian, "Characterising performance of environmental models," *Environ. Model. Softw.*, vol. 40, pp. 1–20, Feb. 2013.
- [66] Y.-L. Chang, A. Anagaw, L. Chang, Y. Wang, C.-Y. Hsiao, and W.-H. Lee, "Ship detection based on YOLOv2 for SAR imagery," *Remote Sens.*, vol. 11, no. 7, p. 786, Apr. 2019.
- [67] G. Cheng, J. Y. Zheng, and M. Kilicarslan, "Semantic segmentation of road profiles for efficient sensing in autonomous driving," in *Proc. IEEE Intell. Vehicles Symp. (IV)*, Jun. 2019, pp. 564–569.
- [68] M. Sun, D. W. Wong, and B. J. Kronenfeld, "A classification method for choropleth maps incorporating data reliability information," *Prof. Geographer*, vol. 67, no. 1, pp. 72–83, Jan. 2015.
- [69] A. Stumpf and N. Kerle, "Object-oriented mapping of landslides using random forests," *Remote Sens. Environ.*, vol. 115, no. 10, pp. 2564–2577, Oct. 2011.
- [70] T. R. Martha, N. Kerle, V. Jetten, C. J. van Westen, and K. V. Kumar, "Characterising spectral, spatial and morphometric properties of landslides for semi-automatic detection using object-oriented methods," *Geomorphology*, vol. 116, nos. 1–2, pp. 24–36, Mar. 2010.
- [71] A. Mayne and R. Perry, "Hierarchically classifying documents with multiple labels," in *Proc. IEEE Symp. Comput. Intell. Data Mining*, Mar. 2009, pp. 170–178.
- [72] W. M. Abdulwahid and B. Pradhan, "Landslide vulnerability and risk assessment for multi-hazard scenarios using airborne laser scanning data (LiDAR)," *Landslides*, vol. 14, no. 3, pp. 1057–1076, Jun. 2017.
- [73] C. J. Tran, O. E. Mora, J. V. Fayne, and M. G. Lenzano, "Unsupervised classification for landslide detection from airborne laser scanning," *Geosciences*, vol. 9, no. 5, p. 221, 2019.
- [74] J. Lu, V. Behbood, P. Hao, H. Zuo, S. Xue, and G. Zhang, "Transfer learning using computational intelligence: A survey," *Knowl.-Based Syst.*, vol. 80, pp. 14–23, May 2015.



BISWAJEET PRADHAN (Senior Member, IEEE)

received the Habilitation degree in remote sensing from the Dresden University of Technology, Germany, in 2011. He is currently the Director of the Centre for Advanced Modelling and Geospatial Information Systems (CAMGIS), Faculty of Engineering and IT. He is also a Distinguished Professor with the University of Technology Sydney. He is also an internationally established Scientist in the fields of geospatial information systems (GIS), remote sensing and image processing, complex modeling/geo-computing, machine learning and soft-computing applications, natural hazards, and environmental modeling. Since 2015, he has been serving as the Ambassador Scientist for the Alexander Humboldt Foundation, Germany. Out of his more than 550 articles, more than 475 have been published in science citation index (SCI/SCIE) technical journals. He has authored eight books and 13 book chapters. He was a recipient of the Alexander von Humboldt Fellowship from Germany. He received 55 awards in recognition of his excellence in teaching, service, and research, since 2006. He was also a recipient of the Alexander von Humboldt Research Fellowship from Germany. From 2016 to 2018, he was listed as the World's Most Highly Cited Researcher by Clarivate Analytics Report as one of the world's most influential mind. In 2018, he was awarded as the World Class Professor by the Ministry of Research, Technology and Higher Education, Indonesia. He is also an Associate Editor and an Editorial Member of more than eight ISI journals. He has widely travelled abroad, visiting more than 52 countries to present his research findings.



HUSAM A. H. AL-NAJJAR received the bachelor's degree in civil engineering and the master's degree in remote sensing and GIS from University Putra Malaysia (UPM), in 2014. He is currently pursuing the Ph.D. degree with the Centre for Advanced Modelling and Geospatial Information Systems (CAMGIS), University of Technology Sydney (UTS). His research interests include the application of deep learning techniques for natural hazard modeling, including landslides, feature extraction from satellite imagery, and UAV-based remote imaging for spatial decision support systems. In 2019, he was awarded the Presidents' Scholarship from UTS. In 2018, he was awarded the International Research Scholarship for the same course. He has several peer-reviewed publications on the application of machine learning methods. He was awarded the Best Paper Award, in 2019, ISPRS Geospatial Week in Enschede, The Netherlands.



MAHER IBRAHIM SAMEEN was born in Dyala, Iraq, in 1990. He received the B.E. degree in surveying engineering from the Technical College of Kirkuk, Iraq, in 2011, and the M.Sc. degree in remote sensing and GIS and the Ph.D. degree in remote sensing from Universiti Putra Malaysia (UPM), Selangor, Malaysia, in 2015. He has participated in many international conferences and published several ISI journal articles. His current research interests include GIS-based modeling, traffic accident analysis, and machine learning. He is currently a Postdoctoral Research Fellow with the School of Information Systems and Modelling, UTS. He is fueled by his passion for developing algorithms for remote sensing and geospatial applications. His background in surveying engineering, geomatics, and remote sensing inform his mindful but competitive approach. He was a recipient of the Best Paper Award of the IEEE Workshop on Geoscience and Remote Sensing (IWGRS 2016), Malaysia.

MUSTAFA RIDHA MEZAAL, photograph and biography not available at the time of publication.



ABDULLAH M. ALAMRI received the B.S. degree in geology from King Saud University, in 1981, the M.Sc. degree in applied geophysics from the University of South Florida, Tampa, in 1985, and the Ph.D. degree in earthquake seismology from the University of Minnesota, USA, in 1990. He is currently a Professor of earthquake seismology and the Director of the Seismic Studies Center, King Saud University (KSU). His research interests include the area of crustal structures and seismic micro zoning of the Arabian Peninsula. His recent projects involve also applications of EM and MT in deep groundwater exploration of Empty Quarter and geothermal prospecting of volcanic Harrats in the Arabian shield. He has published more than 150 research articles, achieved more than 45 research projects as well as authored several books and technical reports. He is a member of Seismological Society of America, American Geophysical Union, European Ass. for Environmental and Engineers, Geophysics, Earthquakes Mitigation in the Eastern Mediterranean Region, National Comm. for Assessment and Mitigation of Earthquake Hazards in Saudi Arabia, Mitigation of Natural Hazards Com at Civil Defense. He is the Principal and a Co-Investigator in several national and international projects (KSU, KACST, NPST, IRIS, CTBTO, US Air force, NSF, UCSD, LLNL, OSU, PSU, and Max Planck). He obtained several worldwide prizes and awards for his scientific excellence and innovation. He has also chaired and co-chaired several SSG, GSF, RELEMR workshops and forums in the Middle East. He is the President of the Saudi Society of Geosciences and the Editor-in-Chief of the *Arabian Journal of Geosciences* (AJGS).

...